Pharm Res (2015) 32:375–388
DOI 10.1007/s11095-014-1468-2

RESEARCH PAPER

Molecularly Imprinted Polymer Nanocarriers for Sustained Release of Erythromycin

Henrik Kempe • Anna Parareda Pujolràs • Maria Kempe

Received: 2 April 2014 / Accepted: 4 July 2014 / Published online: 8 August 2014

ABSTRACT

Purpose To develop and evaluate molecularly imprinted nanocarriers for sustained release of erythromycin in physiological buffer media.

Methods Erythromycin-imprinted *poly*(methacrylic acid–*co*–trimethylolpropane trimethacrylate) nanocarriers and corresponding control nanocarriers were prepared by free-radical precipitation polymerization. The nanocarriers were characterized by transmission electron microscopy, dynamic light scattering, and nitrogen sorption analysis. Binding studies were carried out with erythromycin and five structurally unrelated drugs. Molecular descriptors of the drugs were computed and correlated to measured binding data by multivariate data analysis. Loading with erythromycin and *in vitro* release studies were carried out in physiological buffer media. Kinetic models were fitted to drug release data.

Results The template affected the size and morphology of the nanocarriers. Binding isotherms showed that erythromycin-imprinted nanocarriers had a higher erythromycin binding capacity than corresponding control nanocarriers. Multivariate data analysis, correlating binding to molecular descriptors of the drugs, indicated a molecular imprinting effect. Erythromycin loading capacity was 76 mg/g with a loading efficiency of 87%. Release studies in physiological buffer showed an initial burst release of a quarter of loaded erythromycin during the first day and an 82% release after a week. The release was best described by the Korsmeyer-Peppas model.

Conclusions Sustained release of erythromycin in physiological buffer was demonstrated.

KEY WORDS antibiotics · drug delivery · molecular imprinting · nanoparticles · sustained release

ABBREVIATIONS

AIBN	2,2'-azobisisobutyronitrile
BET	Brunauer, Emmett, and Teller
BJH	Barrett, Joyner, and Halenda
Boc	Tert-butyloxycarbonyl
DLS	Dynamic light scattering
EDMA	Ethylene glycol dimethacrylate
ERY	Erythromycin
HPLC	High-performance liquid chromatography
MAA	Methacrylic acid
MeOH	Methanol
MIP	Molecularly imprinted polymer
NIP	Non-imprinted polymer
PBS	Phosphate buffered saline
Phe	Phenylalanine
PLS	Partial least square
PRESS	Predicted residual sums of squares
RSS	Residual sum of squares
SPE	Solid-phase extraction
TEM	Transmission electron microscope
TFA	Trifluoroacetic acid
TRIM	Trimethylolpropane trimethacrylate
UV	Ultraviolet

INTRODUCTION

Erythromycin (ERY; Structure **1** in Fig. 1) was the first macrolide antibiotic discovered more than 60 years ago. It was isolated from soil samples and was found to be a metabolite of the actinomycete *Saccharopolyspora erythraea*. ERY is used clinically to treat infections of upper and lower respiratory tract, genitals, skin, and soft tissue (1). It has a broader

Electronic supplementary material The online version of this article (doi:10.1007/s11095-014-1468-2) contains supplementary material, which is available to authorized users.

H. Kempe • A. Parareda Pujolràs • M. Kempe (✉)
Nanomedicine and Biomaterials, Department of Experimental Medical Science, Lund University, Biomedical Center, D11, 22184 Lund, Sweden
e-mail: maria.kempe@med.lu.se

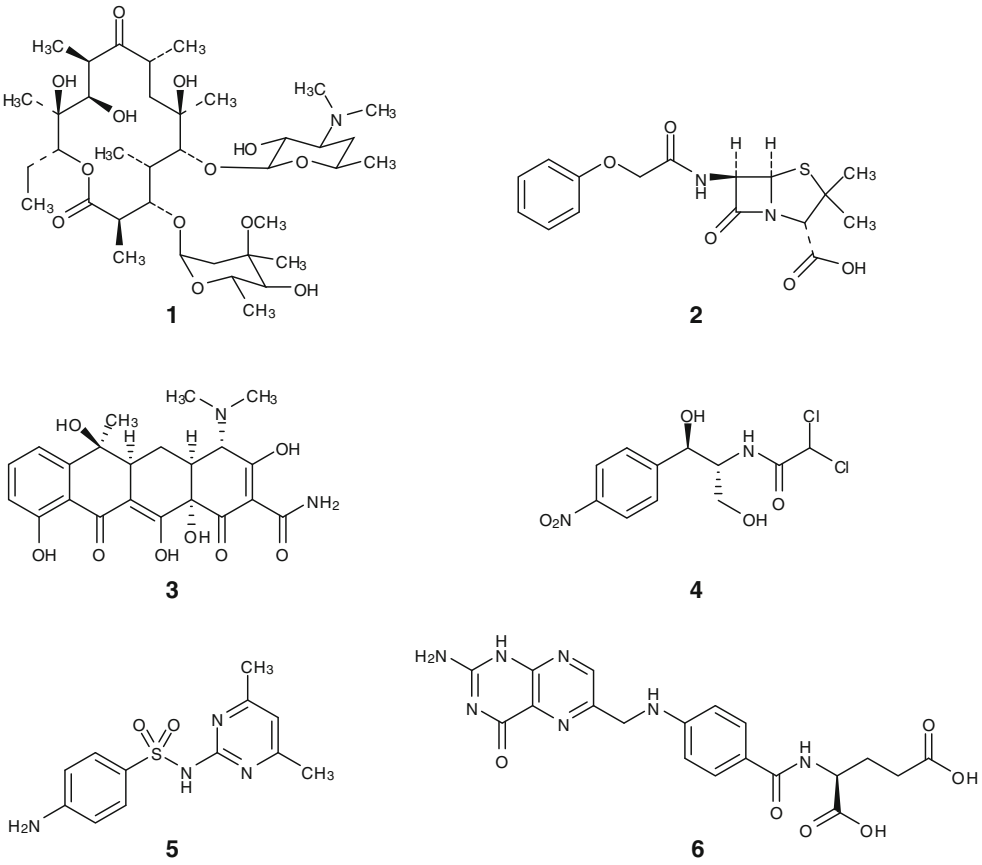

Fig. 1 Structure of erythromycin (**1**), penicillin V (**2**), tetracycline (**3**), chloramphenicol (**4**), sulfamethazine (**5**), and folic acid (**6**).

antimicrobial spectrum than β-lactam antibiotics and is less prone to cause allergic reactions. It is therefore often used as an alternative to β-lactam antibiotics. During the last decades, macrolides have attracted attention not only for their antibacterial activities, but also for their antiinflammatory and immunomodulating effects (2). For example, ERY has been shown to reduce expression of cyclooxygenase-2 in synovial cells from rheumatoid arthritis patients and inhibit periprosthetic tissue inflammation and osteolysis in patients with aseptic loosening (3, 4). Macrolides have been suggested for the treatment of a range of inflammatory conditions including cardiovascular diseases, asthma, cystic fibrosis, diffuse panbronchiolitis, sinusitis, and Crohn's disease (5, 6). The immunosuppressive and antiproliferative effects of non-antibiotic macrolides, *e.g.*, tacrolimus and sirolimus, are utilized at organ transplantations and stent implantations (7, 8).

In light of the increasing number of antibiotic resistant bacterial strains and the challenges related to systemic administration of ERY (*i.e.*, degradation by acid in the stomach, poor absorption, and toxic effects at prolonged treatments), novel therapeutic strategies and dosing regimes are needed. To this end, nanotechnology offers possibilities to provide formulations for targeted and/or sustained drug release. Bosjnakovic *et al.* recently reported on polymer-based dendrimer nanoparticles carrying ERY conjugated via ester bonds (9). The drug payload was 16% by weight and the nanoparticles released 90% of the drug by ester hydrolysis during the first 10 h in phosphate-buffered saline (PBS) at pH 7.4. Doadrio *et al.* reported that functionalization of mesoporous silica nanoparticles with long alkyl chains decreased the release rate of loaded ERY by an order of magnitude compared to the parent non-functionalized nanoparticles (10). The ERY uptake by the nanoparticles was 15% by weight and around 20% was released during the first 10 h in simulated body fluid. Portilla-Arias *et al.* reported on efficient encapsulation of ERY in degradable nanoparticles based on alkyl esters of poly (γ-glutamic acid) (11). The release of the drug followed mainly a polymer-degradation-regulated mechanism during typically 15–40 days. In the present study, we have utilized the method of molecular imprinting to tailor polymeric nanocarriers for sustained release of ERY.

Molecular imprinting is a method that generates recognition sites for a chosen compound (template) in synthetic cross-linked polymers (12, 13). The recognition sites are created by self-assembly of polymer building blocks around the template molecules, followed by fixation of the building blocks by polymerization. The building blocks are typically monomers and cross-linkers of the acrylate, methacrylate or vinyl type. In the non-covalent molecular imprinting approach, the building blocks are chosen so as to provide non-covalent interactions

with the template. Alternatively, the template may be covalently coupled to one or several of the building blocks via cleavable bonds; this approach is referred to as covalent molecular imprinting. Molecularly imprinted polymers (MIPs) have been applied in a broad range of areas, although the majority of studies have focused on the preparation of recognition materials for separation, purification, and analysis. In several cases, drug molecules have been the targets. The use of MIPs for drug delivery has been less studied but is attaining a growing interest. MIPs prepared in various formats, ranging from highly cross-linked micro- and nanoparticles to hydrogels and soft contact lenses, have been evaluated for sustained drug release. In some studies, the MIPs were embedded/incorporated in transdermal adhesives, membranes, tablets, or granules in order to modulate the release kinetics. Several excellent reviews on the potentials of MIPs for drug delivery have been published (14, 15).

We and others have previously prepared molecular recognition elements selective for antibiotics by molecular imprinting (16). Our previous studies focused on β-lactam antibiotic imprinted polymers, prepared either as monolithic polymers, which were subsequently ground to particles, or prepared directly as spherical particles by a surfactant-free suspension polymerization method (17–20). Chloramphenicol, tetracyclines, cephalosporins, sulphonamides, fluoroquinolones, and macrolides are other types of antibiotics that have been subject of interest in molecular imprinting studies (16, 21–28).

The first ERY-imprinted polymer was reported by the Mosbach group in 1997 (24). In this seminal paper on macrolide imprinting, a monolithic MIP was synthesized from methacrylic acid (MAA) and the cross-linker ethylene glycol dimethacrylate (EDMA). The monolith was ground to irregularly shaped micro-sized particles and applied as an HPLC stationary phase for the separation of macrolides using an organic solvent-based mobile phase. The same combination of monomer and cross-linker has been applied in a number of succeeding studies on ERY-imprinted MIPs in both micro- and nano-sized ranges. Song *et al.* followed a similar procedure as the Mosbach group for the preparation of irregularly shaped ERY-imprinted microparticles and Geng *et al.* prepared microspheres by suspension polymerization (25, 26). In both studies, the MIPs were applied as a sorbent for solid-phase extraction (SPE) of ERY from methanol–water mixtures. In addition, Song *et al.* tested, with poor results, the cross-linker trimethylolpropane trimethacrylate (TRIM) for the imprinting of ERY by bulk co-polymerisation with MAA (25). A plausible explantion of the discouraging results may be the use of sub-optimal molar ratios of the building blocks. When we introduced TRIM as a cross-linker for the preparation of MIPs in the mid 1990s, optimal selectivity and binding capacity were obtained with equimolar amounts of MAA and TRIM (29, 30). An aim of the present study was to test these conditions for the imprinting of ERY. Another reason for the poor performance of the TRIM-cross-linked MIPs in the study by Song *et al.* may be the choice of a methanol–acetonitrile mixture as the porogen. This solvent mixture may interfere with the self-assembly process in the pre-polymerization mixture. In the present study, we have chosen acetonitrile as the porogen as this solvent have previously been used successfully with a range of templates.

Sub-micron sized MIPs are not readily prepared by neither suspension polymerisation nor grinding of monolithic polymers. Kou *et al.* recently reported on the preparation of sub-micron-sized ERY-imprinted MIP spheres by precipitation polymerization (27), a method initially pioneered for imprinting by the Mosbach group (31). The spheres, prepared from MAA and EDMA, had an average diameter of about 550 nm. Zhang *et al.* reported on a conceptually different approach: MAA, EDMA, and acryloyl-β-cyclodextrin were polymerized on the surface of multi-walled carbon nanotubes (28). The composite nanoparticles,were applied as a sorbent for SPE of ERY from a methanol–water mixture.

As described above, previous ERY-imprinted polymers were developed for re-binding in media containing organic solvents. To the best of our knowledge, no studies have reported on binding of ERY in pure water-based media. For biological applications it is required that the MIPs can operate under physiological conditions. The aim of the present study was to evaluate the usefulness of TRIM for the development of ERY-imprinted nanoparticles capable of sustained drug release in physiological pH-buffered saline solutions.

MATERIALS AND METHODS

Materials

Methacrylic acid (MAA), trimethylolpropane trimethacrylate (TRIM), (−)-erythromycin hydrate (96%), penicillin V (free acid, 99.8%), tetracycline (min. 95%), chloramphenicol (98%), sulfamethazine (99%), and folic acid (98%) were purchased from Aldrich (Milwaukee, WI, USA). 2,2′-Azobisisobutyronitrile (AIBN) was obtained from Acros (Geel, Belgium). MAA was purified by distillation and AIBN was recrystallized from methanol (MeOH) prior to use. P.a. grades of acetonitrile (CH_3CN) and MeOH, used for the synthesis and extraction of the polymers, were purchased from Merck (Darmstadt, Germany). Acetic acid was of grade "anhydrous for analysis" from Merck. CH_3CN, used for the HPLC analyses, were of grade "HPLC far UV" from Labscan (Dublin, Ireland). Phosphate-buffered saline pH 7.4, PBS (10 mM phosphate buffer, 2.7 mM potassium chloride, and 137 mM sodium chloride) was prepared from tablets obtained from Sigma (St Louis, MO, USA).

Synthesis of Nanocarriers

ERY (0.294–0.734 g, 0.4–1 mmol) and MAA (0.344 g, 4 mmol) were dissolved in 4.5 ml of CH_3CN by sonication in an ultrasonic bath. TRIM (1.356 g, 4 mmol) and AIBN (0.938 g, 5.7 mmol) were added and the mixture was again sonicated. The solution was diluted with 35.5 ml of CH_3CN, cooled on ice, and purged with nitrogen gas for 5 min. Precipitation polymerization was carried out in a water bath at 60°C for 8 h. After polymerization, the sample was centrifuged (9,500 rpm, 3 h) and the supernatant was discarded. The MIP nanocarriers were extracted in sequence with MeOH–acetic acid (1:1, v/v), MeOH, water, and MeOH. Extractions were carried out three times with each solvent and included first sonication in an ultrasonic bath (3 h) and then an overnight incubation on a VXR basic Vibrax shaking table (IKA-Werke, Staufen, Germany) set at 1,000 rpm. Between incubations, the sample was centrifuged (9,500 rpm, 3 h) and the supernatants were discarded. Finally, the nanocarriers were dried *in vacuo* overnight. Control nanocarriers, imprinted with Boc-phenylalanine (Boc-Phe-MIP) and non-imprinted polymer (NIP), were prepared with Boc-phenylalanine (0.133 g, 0.5 mmol) as the template and without a template, respectively, following the procedure described above for the preparation of ERY-imprinted MIP nanocarriers. Compositions of all nanocarriers are summarized in Table I. The yields of the final dried nanocarriers were typically 1.25–1.5 g.

Physical Characterization of Nanocarriers

Hydrodynamic particle size distribution of the final nanocarriers (100 μg per ml of water) was determined by dynamic light scattering (DLS) using a Nanotrac Ultra Particle Size Analyzer from Microtrac (Montgomeryville, PA, USA). Each measurement was carried out for 60 s. The reported data are the mean values of ten measurements. The size growth of the ERY-MIP nanocarriers during the polymerization was followed by DLS analysis. Samples were withdrawn from the polymerization mixture at different time points and diluted ten times with CH_3CN.

Size and morphology of dry nanocarriers were imaged with a FEI Tecnai Spirit Biotwin transmission electron microscope (TEM) (Hillsboro, OR, USA). Nanocarriers were deposited onto carbon film grids by pipetting a drop (approx. 10 μl) of nanocarrier solution (100 μg/ml) onto the grid. The nanocarriers were allowed to settle and excess solution was removed by contacting a filter paper to the edge of the grid. The grid was allowed to dry at room temperature prior to insertion into the TEM vacuum chamber.

Surface area and porosity were determined by nitrogen gas sorption analysis using an ASAP 2,400 analyzer (Micromeritics Instrument Corporation, Norcross, GA, USA). The nanocarrier samples were pretreated by applying vacuum at 30°C for 2 days. The adsorption and desorption isotherms were recorded using 80-point pressure tables with 20-s equilibration intervals. The method of Brunauer, Emmett, and Teller (BET) was used to calculate the surface area using a model of adsorption involving multilayer coverage. The method of Barrett, Joyner, and Halenda (BJH) was used to calculate the size distributions of meso- and macropores using the Kelvin model of pore filling. The deBoer t-plot method was used to determine the external surface area and the micropore volume. The average pore diameter was calculated as 4×(total pore volume)/(BET surface area).

Study On Influence of ERY-MIP Nanocarrier Formulation on Binding Capacity

Triplicate samples (5 mg) of ERY-MIP nanocarriers, prepared with ERY to MAA ratios of 1:4, 1:6, 1:8, and 1:10, and NIP nanocarriers (Table I) were incubated with 1 mL of ERY (0.5 mM) in PBS for 18 h in micro-centrifuge tubes on a shaking table (1,500 rpm). After centrifugation (1 h, 13,000 rpm), the supernatants were withdrawn and analyzed by high-performance liquid chromatography (HPLC) on a Waters system comprising a model 600 Multisolvent Delivery Module, a model 600 Pump, and a model 2487 Dual Wavelength Absorbance Detector. An ACE3 C18 column (150×4.6 mm) from Advanced

Table I Composition of Nanocarriers

Nanocarrier	Template	Amount				
		Template (mmol)	MAA (mmol)	TRIM (mmol)	AIBN (mmol)	CH_3CN (mL)
ERY-MIP (template–MAA, 1:4)	ERY	1	4	4	5.7	40
ERY-MIP (template–MAA, 1:6)	ERY	0.667	4	4	5.7	40
ERY-MIP (template–MAA, 1:8)	ERY	0.5	4	4	5.7	40
ERY-MIP (template–MAA, 1:10)	ERY	0.4	4	4	5.7	40
Boc-Phe-MIP (template–MAA, 1:8)	Boc-Phe-OH	0.5	4	4	5.7	40
NIP	–	–	4	4	5.7	40

Chromatography Technologies (Aberdeen, Scotland) was used as the stationary phase. The flow rate was 1 ml/min. ERY was eluted with acetonitrile–50 mM sodium phosphate buffer pH 6.3 (35:65, *v/v*) and detected at 214 nm. Absorbance data were acquired via a PC by Chromatography Station for Windows software (DataApex, Prague, Czech Republic). The bound amounts of ERY to ERY-MIP and NIP nanocarriers (i.e., $N_{ERY\text{-}MIP}$ and N_{NIP}), respectively, were determined. The specific binding of ERY to each ERY-MIP nanocarrier was calculated by subtracting the measured amount bound to the NIP nanocarriers from the amount bound to each ERY-MIP nanocarrier (i.e., $N_{Spec.\ ERY\text{-}MIP}=N_{ERY\text{-}MIP} - N_{NIP}$). The theroretical number of template molecules present in each of the MIP nanocarriers during the imprinting process ($N_{Template\ ERY\text{-}MIP}$) was then calculated from nanocarrier synthesis data. Finally, the fraction of theroretical number of recognition sites occupied by ERY during the rebinding (F) was calculated as $F=N_{Spec.\ ERY\text{-}MIP}/N_{Template\ ERY\text{-}MIP}$.

Saturation Binding Isotherms

Triplicate samples of nanocarriers (5 mg) were incubated with 1 ml of increasing concentrations of ERY (0.05–0.5 mM) in PBS for 18 h in micro-centrifuge tubes on a shaking table (1,500 rpm). After centrifugation (1 h, 13,000 rpm), the supernatants were withdrawn and analyzed by HPLC as described above. One-site Langmuir isotherms were fitted to calculated binding data using GraphPad Prism 4.0b (GraphPad Software, Inc., San Diego, CA, USA).

Studies on Binding of ERY, Penicillin V, Tetracycline, Chloramphenicol, Sulfamethazine, and Folic Acid to Nanocarriers

Nanocarriers (5 mg/ml PBS) and drug (ERY, penicillin V, tetracycline, chloramphenicol, sulfamethazine, or folic acid; 0.5 mM), dissolved in PBS, were incubated in micro-centrifuge tubes on a shaking table for 20 h at room temperature. All experiments were carried out in triplicate. After centrifugation (2 h, 13,000 rpm), the supernatants were analyzed by HPLC (ERY, penicillin V, tetracycline, and chloramphenicol) or UV spectrophotometry (sulfamethazine and folic acid). HPLC analysis of ERY was carried out as described above. Penicillin V was eluted with water–acetonitrile–TFA (700:300:1) and detected at 260 nm. Tetracycline and chloramphenicol were eluted with water–acetonitrile–TFA (850:150:1, *v/v/v*) and detected at 260 nm. UV spectrophotometry was carried out at 261 nm (sulfamethazine) and 434 nm (folic acid) using a Lambda XLS+spectrophotometer from Perkin Elmer (Beaconsfield, UK). The concentration of free drug in the supernatant was determined and the percentage of drug bound to the nanocarriers (% B) was thereafter calculated.

Molecular Computations

Two-dimensional structures of the drugs were constructed with ChemDraw Ultra 10.0 of the ChemOffice 2006 software package (CambridgeSoft, Cambridge, MA, USA). The structures were imported into Chem 3D Ultra 10.0 to obtain three-dimensional structures. The energy of the structures was minimized first by a modified version of Allinger's MM2 force field and then by the semiempirical molecular orbital MOPAC algorithm with the Austin model 1 Hamiltonian approximation. Closed shell wave function, the Eigenvector Following (EF) geometry optimization routine, and H_2O as the solvent were applied. The following molecular descriptors were then calculated with the MOPAC application and the ChemProp interface: core-core repulsion, COSMO area, COSMO volume, dipole, electronic energy, heat of formation, ionization potential, molecular weight, total energy, Connolly accessible area, Connolly molecular area, Connolly solvent excluded volume, ovality, molecular refractivity, partition coefficient, Balaban index, cluster count, molecular topological index, number of rotatable bonds, polar surface area, radius, shape attribute, sum of degrees, sum of valence degrees, topological diameter, total connectivity, total valence connectivity, and Wiener index. The Connolly accessible area, the Connolly molecular area, the Connolly solvent excluded volume, and the ovality were calculated with a probe radius of 0.001 Å (*i.e.*, the minimum radius permitted by the software) (32).

Correlation of Binding Data and Molecular Descriptors by Multivariate Data Analysis

To correlate the percentage of drug bound to the nanocarriers (% B) to the molecular descriptors, multivariate data analysis was carried out by partial least square (PLS) regression using the Simca-P 8.0 software (Umetrics AB, Umeå, Sweden). The software automatically mean-centered and scaled the data to unit variance prior to modeling and determined the number of significant components by cross-validation. Cross-validation was carried out by calculating and comparing the predicted sum of squares (PRESS) for each model dimension with the residual sum of squares (RSS) of the previous dimension. A component was considered significant when PRESS was significantly smaller than RSS.

Drug Loading and Release Studies

ERY-MIP nanocarriers (7.5 mg/ml) were incubated with ERY (1 mM) in PBS on a shaking table (1,500 rpm) for 20 h in room temperature. After incubation, the mixture was centrifuged

(9,500 rpm, 1 h), the supernatant was removed, and the nanocarriers were dried *in vacuo* overnight. The supernatant was analyzed by HPLC as described above to determine the free concentration of ERY. The amount of ERY bound to the nanocarriers was thereafter calculated.

Drug release experiment under sink conditions was initiated by immersing 50 mg of ERY-loaded nanocarriers (freshly dispersed in 1 ml of PBS), contained in a Spectra/Por dialysis tube membrane (MW cut off 6–8 kDa, flat width 10 mm, ∅ 6.4 mm; Spectrum Laboratories Inc., Rancho Dominguez, CA, USA), into a volume of 500 ml of PBS. The experiment was carried out at room temperature and the buffer solution was stirred with a magnetic stirrer. Triplicate 10-ml samples of the buffer solution were withdrawn periodically and replaced with fresh PBS. Withdrawn samples were lyophilized to dryness, reconstituted in 0.5–1 ml of water, and analyzed by HPLC as described above. Kinetic models were fitted to the released amounts of ERY using the GraphPad Prism software.

RESULTS AND DISCUSSION

Nanocarrier Synthesis and Physical Characterization

Nanocarriers were synthesized by free-radical precipitation polymerization of MAA and TRIM in acetonitrile. ERY was used as a template during the polymerization in order to create recognition sites for the drug in the polymer network of the resulting nanocarriers. MAA is one of the most commonly used functional monomers for the preparation of MIPs and has been applied to the imprinting of a broad range of templates. It was assumed that MAA would interact with ERY via hydrogen bonds and ionic interactions as previously reported (25). The general strategy in molecular imprinting is to co-polymerize the functional monomers with cross-linkers. The main role of the cross-linker is to provide rigidification of the monomer-template assemblies present in the pre-polymerization mixture, although examples of functionalized cross-linkers that interact directly with the template, making functional monomers redundant, have been reported (33). TRIM has emerged as a frequently used cross-linking component of MIPs after its introduction into the field two decades ago (27, 28). Based on optimizations in our previous studies (27, 28) a MAA to TRIM ratio of 1:1 was applied in this study.

The co-polymerizations, initiated by thermolytic homolysis of AIBN, were allowed to proceed for up to 8 h at 60°C. Heat-induced homolysis was selected over UV-induced homolysis, since ERY has been reported to be photoreactive (34). Initial experiments carried out with a low concentration of AIBN (*i.e.*, 4.7 mg of AIBN per ml of added acetonitrile) were slow and particles were not detected by DLS until the polymerization had proceeded for 2 h (Fig. 2a). It has previously been reported that the polymerization rate depends on the square root of the concentration of AIBN (35). The concentration of AIBN was therefore increased to improve the polymerization rate. A five times higher AIBN concentration gave a substantially faster particle growth (Fig. 2a). The higher concentration of AIBN was therefore chosen for the remaining studies. Figure 2b shows that the particle size increased and the size distribution became broader during the time course of the polymerization. After the polymerization, the nanocarriers were retrieved by centrifugation, subjected to liquid extraction with solvents to remove template molecules and any unreacted reagents, and finally dried *in vacuo*. All of the nanocarriers prepared showed good chemical, physical, and mechanical stability and were stored in the dried state at room temperature for several years with retained performance.

The amount of acetonitrile added to the polymerization mixture was found to be another influential parameter for the

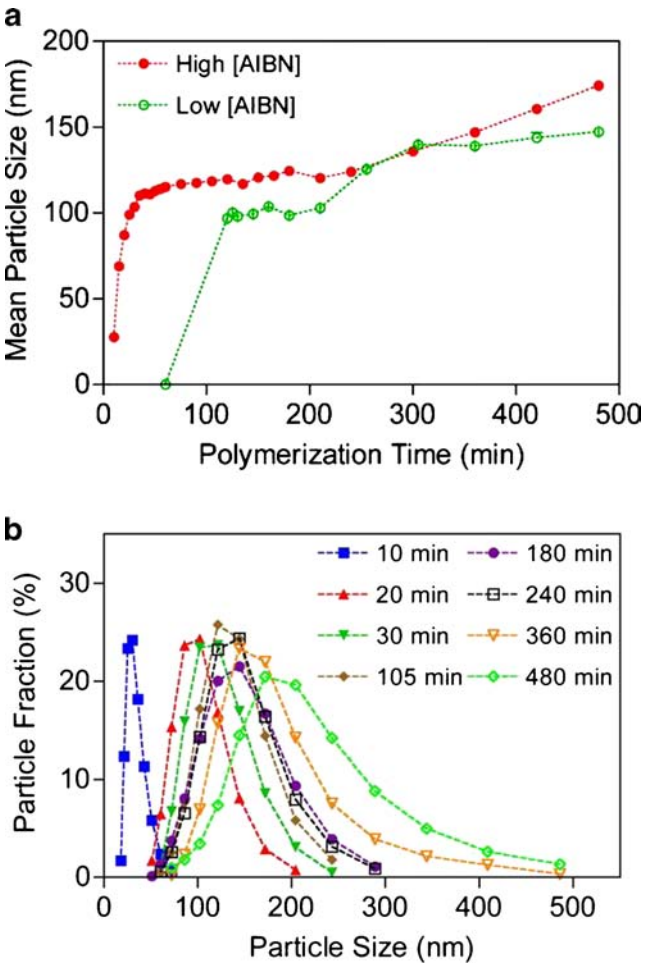

Fig. 2 ERY-MIP nanocarrier growth during precipitation polymerization. Nanocarriers were prepared with an MAA/ERY ratio of 8. (**a**) Mean particle size determined by DLS during polymerization with low (*green*) and high (*red*) concentration of the initiator AIBN (i.e., 4.7 and 23.4 mg AIBN/ml CH_3CN, respectively). Error bars denote standard errors. (**b**) Particle size distribution determined by DLS during polymerization with high concentrations of AIBN.

precipitation of nanoparticles in high yield. The initial conditions applied (*i.e.*, 10 ml of acetonitrile per mmol of TRIM), gave nanoparticles in acceptable yields. Decreasing the volume of acetonitrile by 50% resulted in the formation of a monolithic polymer gel that filled up the total polymerization volume. Increasing the volume by 50% or more resulted in smaller sized nanoparticles (<100 nm) obtained in substantially lower yield. The amount of acetonitrile was kept at the initial conditions for the remaining studies.

The functional monomer, in this case MAA, is instrumental to the formation of template-polymer interactions and the creation of selective recognition sites in the MIP network. The influence of MAA on the binding capacity of the resulting nanocarriers was investigated on a panel of ERY-MIP nanocarriers formulated with 4, 6, 8, and 10 equivalents, respectively, of MAA per equivalent of ERY (Table I). The study was designed so that the amount of ERY added to the polymerization mixtures during the preparation of the nanocarriers was varied while the remaining components were kept constant. This was to ensure that all nanocarriers had identical polymer composition and differed only in the amount of ERY present during the formation of the recognition sites. Non-imprinted polymer (NIP) nanocarriers of identical composition was also prepared. After extraction of ERY, the binding capacity of the nanocarriers was investigated by incubation with ERY. The measured binding of ERY to the NIP nanocarriers was subtracted from the measured binding of ERY to the four different ERY-MIP nanocarriers to calculate the specific binding to each ERY-MIP nanocarrier. These values were then related to the amount of template added to each preparation during the imprinting polymerization, i.e., to the theoretical number of recognition sites that could have formed in each nanocarrier sample if all ERY molecules were imprinted successfully. Hence, the fraction of theoretical number of recognition sites occupied during the rebinding was calculated and used as a measure of the imprinting efficiency. As seen in Fig. 3, the fraction leveled out at an MAA to ERY ratio of 8. This ratio was therefore applied to all nanocarriers for the remaining studies.

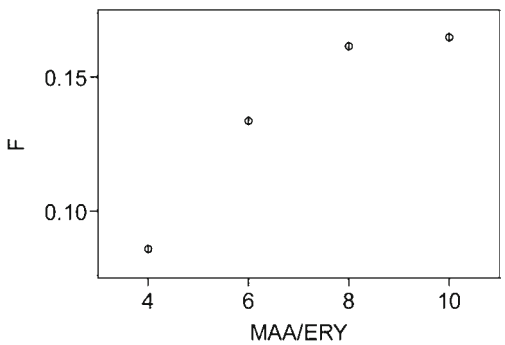

Fig. 3 Influence of MAA/ERY ratio on the fraction of theoretical number of recognition sites occupied by ERY during the rebinding (F).

Control nanocarriers were prepared following the procedure for the preparation of the ERY-MIP nanocarriers. The purpose of control polymers in the evaluation of MIPs is to verify that the imprinting procedure has produced recognition sites for the template in the imprinted polymer network, *i.e.*, to verify the existence of an imprinting effect. The choice of polymers used as controls has been subject to some debate. MIPs often have a higher surface area than corresponding non-imprinted polymers, NIPs (36). A higher surface area may result in a larger (non-selective) binding capacity. Another consideration is the influence of functional monomer dimerization on the binding capacity of the final polymer (37). In MAA, mutual hydrogen bonding from the OH group of one molecule to the carboxyl oxygen of another is responsible for the dimer formation. This means that a portion of the MAA molecules present in the pre-polymerization mixture may form dimers. After polymerization, the functional groups are locked in a position that promotes sustained dimer interactions. This effect is more pronounced in NIPs than in MIPs, since a substantial portion of the functional monomers present in the pre-polymerization mixtures of the latter are involved in interactions with the template molecules. After extraction of the templates, the functional groups originating from MAA become exposed and free to interact with incoming molecules during rebinding. Hence, both differences in surface area and functional monomer dimerization are factors that may overestimate the imprinting effect of MIPs in comparative studies with NIPs. Despite this, the majority of molecular imprinting studies to date have assessed the binding of MIPs by comparisons with NIPs and the observed binding differences have been ascribed to an imprinting effect and the presence of recognition sites. To prevent an overestimation of the imprinting effect, control polymers imprinted with a template that is structurally different from the target molecule may be used. In this study, control polymers were prepared by substituting Boc-phenylalanine for ERY and by omitting the template, resulting in Boc-Phe-MIP and NIP (non-imprinted) nanocarriers, respectively. As a further precaution to prevent overestimation of the imprinting effect, a binding study with a small library of structurally unrelated drug molecules were carried out (discussed below).

DLS analysis of the final nanocarriers in water showed an apparent mean hydrodynamic diameter of approximately 152 nm of both the ERY-MIPs and the NIPs whereas the Boc-Phe-MIP nanocarriers were almost twice as large (Fig. 4; Table II). Similar values were obtained when the nanocarriers were dispersed in acetonitrile (Table II). Imaging of the ERY-MIP nanocarriers by TEM showed a complex morphology; the micrographs show aggregates or clusters with an apparent knotted worm- or network-like structure (Fig. 5a and b). The mean size of the "knots" in the micrograph in Fig. 5a is 43 nm and the mean size of the "worms" is 173 nm. The precipitation polymerization was repeated several times to ensure that

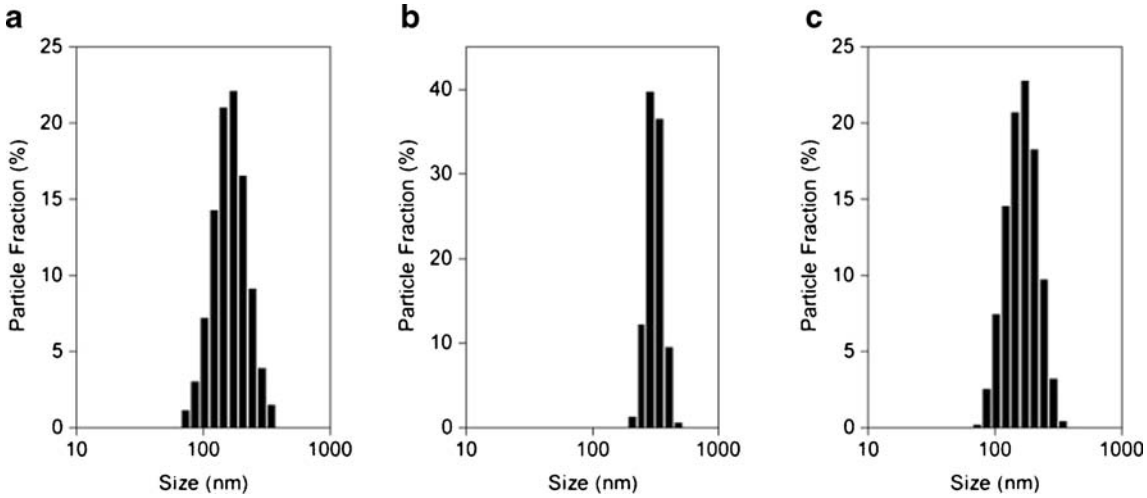

Fig. 4 Particle size distribution determined by DLS analysis. (**a**) ERY-MIP nanocarriers (prepared with an MAA/ERY ratio of 8), (**b**) Boc-Phe-MIP nanocarriers (prepared with an MAA/Boc-Phe-OH ratio of 8), and (**c**) NIP nanocarriers.

the observed morphology was representative; all preparations showed the same morphology by TEM. TEM of ERY-MIP nanocarriers retrieved after 2 h of polymerization showed the same morphology as well. It is unclear if the observed morphology was due to distortion and aggregation during the polymerization, during the work-up steps, or during the deposition of the particles onto the TEM carbon film grids.

The larger diameter of the Boc-Phe-MIP nanocarriers, as determined by DLS, was confirmed by TEM, which showed a mean diameter of 189 nm of the dried nanocarriers (Fig. 5c). The mean diameter of the dried NIP nanocarriers according to TEM was 80 nm (Fig. 5d). Hence, the size and morphology of the nanoparticles formed during the precipitation polymerization was dependent on the presence/absence of template as well as the nature of the template. This same phenomenon has been noted previously by several researchers. Cacho *et al.* reported that micro-sized MIPs prepared by precipitation polymerization in presence of the template fenuron were of uniform size whereas MIP particles prepared in presence of propazine acting as the template were agglomerated and polydisperse (38). Likewise, Chen and Ye noted that nanoparticles prepared by precipitation polymerization in presence of propranolol were of uniform size while atrazine-imprinted nanoparticles, prepared according to the same procedure, were larger and had a very broad size distribution (39). The latter authors suggested that the template affects the process of particle nucleation and growth.

The BET surface area, the Langmuir surface area, the BJH adsorption and desorption areas, the external surface area,

Table II Characteristics of Nanocarriers[a]

	ERY-MIP	Boc-Phe-MIP	NIP
Mean hydrodynamic diameter by DLS (nm) in water	152 ± 3 (n = 10)	288 ± 7 (n = 10)	152 ± 2 (n = 10)
Mean hydrodynamic diameter by DLS (nm) in CH_3CN	146 ± 1 (n = 10)	296 ± 4 (n = 10)	135 ± 1 (n = 10)
Mean diameter by TEM (nm)	knots: 43 ± 1 (n = 50) aggregates: 173 ± 25 (n = 30)	189 ± 7 (n = 44)	80 ± 1 (n = 190)
BET surface area (m^2/g)	157	27	34
Langmuir surface area (m^2/g)	218	38	47
BJH adsorption area (m^2/g)	127	20	24
BJH desorption area (m^2/g)	139	21	26
External surface area (m^2/g)	121	23	27
Micropore area (m^2/g)	36	4	7
Average pore diameter (nm)	16	17	19
Total pore volume (ml/g)	0.62	0.11	0.16
Micropore volume (ml/g)	0.0139	0.0014	0.0022

[a] ± values are standard errors

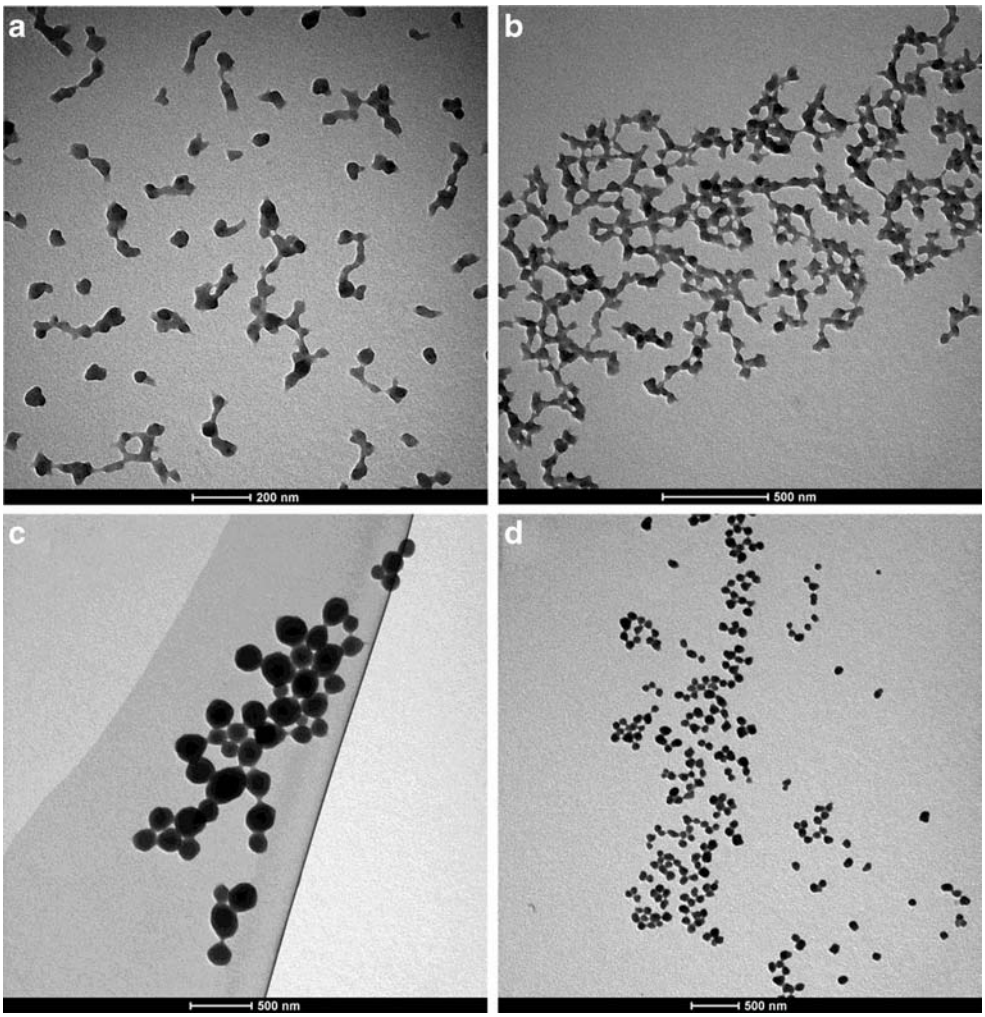

Fig. 5 Transmission electron micrographs of (**a**,**b**) ERY-MIP nanocarriers (prepared with an MAA/ERY ratio of 8), (**c**) Boc-Phe-MIP nanocarriers (prepared with an MAA/Boc-Phe-OH ratio of 8), and (**d**) NIP nanocarriers.

and the micropore area (*i.e.*, the area of pores with a diameter <2 nm), all calculated from the nitrogen gas sorption isotherms (Fig. 6), were higher for the ERY-MIP nanocarriers than for the control nanocarriers (Table II). It is well known that the total external surface area of a sample increases with decreasing size of particles. The smaller size of the ERY-MIPs compared to the control particles therefore explain, at least partly, the larger surface area. The isotherms of the ERY-MIP nanocarriers show some hysteresis (Fig. 6a), suggesting the presence of mesopores (*i.e.*, pores in the size range 2–50 nm). The pore volume vs. pore size plots of the ERY-MIP nanocarriers in Fig. 7, calculated from the desorption isotherm using the BJH model, shows a peak at a pore diameter of 23 nm. The corresponding plots of the control nanocarriers in Fig. 7 do not indicate any mesopores, but shows the presence of macropores (*i.e.*, pores >50 nm). The total pore volume and the micropore volume of the ERY-MIP nanocarriers were four to ten times higher than the corresponding volumes of the control nanocarriers (Table II). The average diameter of the pores of the NIP nanocarriers was slightly larger (13–21%) than those of the imprinted nanocarriers (Table II). Summarizing, the data shows that the presence and nature of the template affects both porosity and surface area.

Binding Studies

One-site Langmuir binding isotherms of ERY, obtained in PBS, showed that the ERY-MIP nanocarriers had a higher ERY binding capacity than the control nanocarriers (Fig. 8). The number of binding sites calculated from the isotherms was 87 μmol per gram of ERY-MIP nanocarriers. The corresponding data for the control nanocarriers were 30 and 44 μmol per gram of Boc-Phe-MIP and NIP nanocarriers, respectively.

The observed two to three times higher ERY binding capacity of the ERY-MIP nanocarriers compared to the control polymer nanocarriers may (i) originate from an imprinting effect formed by ERY molecules present during the polymerization and/or (ii) be due to an increased non-specific adsorption due to the larger surface area of the ERY-MIP nanocarriers. The former hypothesis assumes that binding

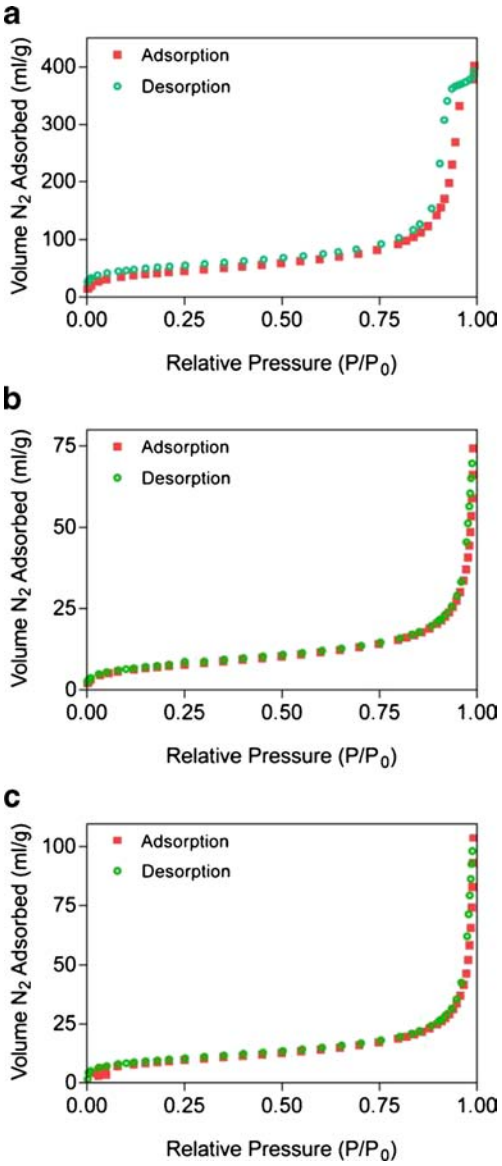

Fig. 6 Nitrogen adsorption (*red*) and desorption isotherms (*green*) on (**a**) ERY-MIP nanocarriers (prepared with an MAA/ERY ratio of 8), (**b**) Boc-Phe-MIP nanocarriers (prepared with an MAA/Boc-Phe-OH ratio of 8), and (c) NIP nanocarriers.

sites are formed throughout the polymer network during the polymerization and that these sites later are accessible for rebinding of ERY; this is in fact the general understanding of the concept of molecular imprinting. The latter hypothesis, on the other hand, takes into consideration that the ERY-MIP nanocarriers have a four to six times larger surface area than the control nanocarriers (as shown by the nitrogen sorption analysis above). A binding mechanism based solely on non-specific surface adsorption would therefore, under optimal binding conditions, result in a higher binding capacity of the ERY-MIP nanocarriers due to their larger surface area. Such a mechanism is expected, however, to reflect in increased binding of not only ERY but also of other compounds.

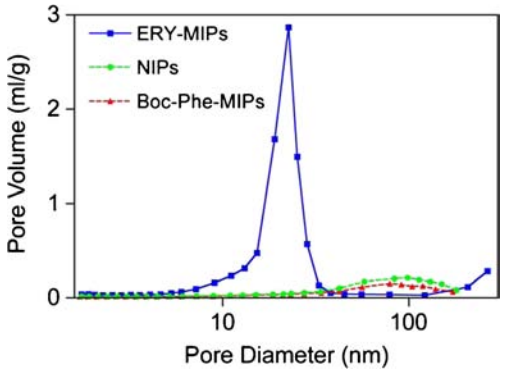

Fig. 7 Pore volume vs. pore size plots of ERY-MIP nanocarriers prepared with an MAA/ERY ratio of 8 (*blue*), Boc-Phe-MIP nanocarriers prepared with an MAA/Boc-Phe-OH ratio of 8 (*red*), and NIP nanocarriers (*green*) calculated from the nitrogen desorption isotherms using the BJH model.

The general adsorptive capacity of the ERY-MIP and the NIP nanocarriers was investigated in a binding study that included a small library of structurally unrelated drug molecules, namely erythromycin, penicillin V, tetracycline, chloramphenicol, sulfamethazine, and folic acid (Structures in Fig. 1; binding results in Fig. 9). Consistent with both the saturation binding isotherms (Fig. 8) and the expected enhanced binding originating from an imprinting effect, the study showed significantly higher binding of ERY to the MIP nanocarriers than to the NIP nanocarriers. The study also showed a considerable binding of both chloramphenicol and sulfamethazine to both the ERY-MIP nanocarriers and the control nanocarriers; the binding was in fact higher to the control nanocarriers than to the ERY-MIP nanocarriers in both cases. The results suggest that the binding is of non-specific nature and that neither chloramphenicol nor sulfamethazine are recognized by the imprinted recognition sites of the ERY-MIP nanocarriers. The binding of tetracycline was moderate, but higher to the ERY-MIP nanocarriers than to the NIP control nanocarriers. The results suggest that some of the recognition sites of the ERY-MIP nanocarriers may be

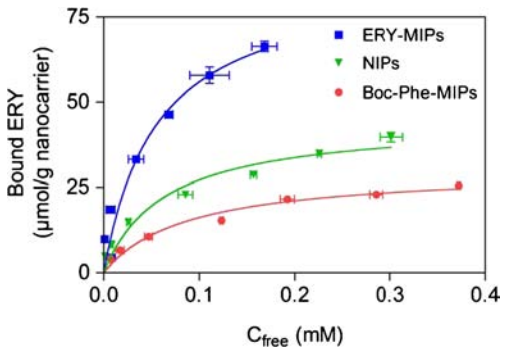

Fig. 8 One-site Langmuir binding isotherms of ERY to ERY-MIP nanocarriers prepared with an MAA/ERY ratio of 8 (*blue*), Boc-Phe-MIP nanocarriers prepared with an MAA/Boc-Phe-OH ratio of 8 (*red*), and NIP nanocarriers (*green*). Binding was carried out in PBS (pH 7.4) at ambient temperature. Error bars denote standard errors.

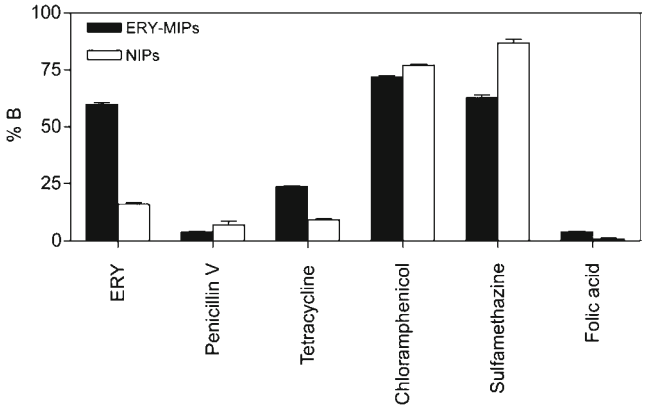

Fig. 9 Percentage of drugs bound (% B) to ERY-MIP nanocarriers prepared with an MAA/ERY ratio of 8 (*black bars*) and NIP nanocarriers (*white bars*). Error bars denote standard errors.

accessible to tetracycline. Only small amounts of added penicillin V and folic acid bound to either of the nanocarriers. Hence, the results did not show conclusively that the higher surface area of the ERY-MIP nanocarriers resulted in an overall higher binding compared to the NIP nanocarriers.

Non-specific binding to the nanocarriers may take place via various interactions (*e.g.*, hydrogen bonds, ionic interactions, and hydrophobic interactions), depending on the binding conditions and the nature of the drug molecule and the polymer. To investigate the binding mechanism further while taking the nature of the bound drug molecules into account, the binding/adsorption of the drugs to the nanocarriers was correlated by multivariate data analysis to molecular descriptors of the respective drugs. The energy of the drug molecules was first minimized by semiempirical quantum mechanical methods to obtain stable three-dimensional conformations. Twenty-eight molecular descriptors of each drug were thereafter computed. PLS regression was carried out on all observations (*i.e.*, the six drugs included in the library) using the full data set, comprising the percentage of added drug that bound to the nanocarriers (*i.e.*, the **Y** matrix) and the 28 descriptors for each drug (*i.e.*, the **X** matrix). The analysis of the NIP nanocarriers resulted in a three-component model that used 90.5% of the *x* variation to describe 99.7% and predict 86.2% of the *y* variance (Table SI in Supplementary Materials). Figure 10b shows that there is a good correlation between the observed and the predicted binding, suggesting that the all of the drugs bound through a similar binding mechanism to the NIP nanocarriers.

A corresponding PLS regression analysis using the binding data obtained on the ERY-MIP nanocarriers failed to correlate the binding data and the descriptors when all of the drugs were included. When ERY was omitted from the data set, a two-component model that used 83.1% of the *x* variation to describe 99.9% and predict 74.0% of the *y* variation was obtained (Table SI in Supplementary Materials). Figure 10a shows the observed vs. predicted binding to the ERY-MIP

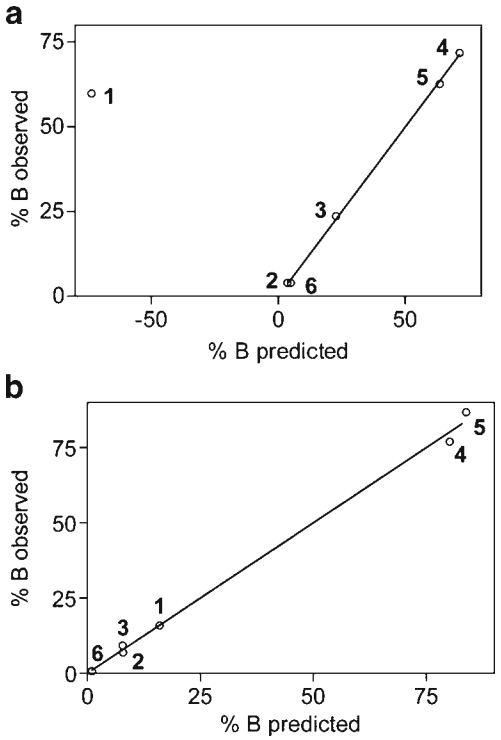

Fig. 10 Plot of observed vs. predicted percentage bound (% B) of ERY (**1**), penicillin V (**2**), tetracycline (**3**), chloramphenicol (**4**), sulfamethazine (**5**), and folic acid (**6**) to (a) MIP nanocarriers prepared with an MAA/ERY ratio of 8 and (b) NIP nanocarriers.

nanocarriers. The observed binding of ERY was significantly higher than predicted by the model. Hence, ERY did not fit the model and the binding was not explained by its molecular descriptors. The results support the hypothesis that the observed higher binding of ERY to the ERY-MIP nanocarriers, as compared to the control nanocarriers, was due to a molecular imprinting effect that created recognition sites of ERY in the polymer network.

Drug Loading and Release Studies

Drug loading was carried out by incubating the nanocarriers with ERY in PBS during 20 h. The nanocarriers were thereafter separated from the solution by centrifugation and dried *in vacuo*. The drug loading efficiency was 87% and the loading capacity was 76 mg of ERY per gram of nanocarriers. Release of ERY was studied under sink conditions by placing the nanocarriers in a dialysis tube, which was immersed into a gently stirred release media consisting of PBS pH 7.4. At predetermined time points, triplicate samples of the release media were withdrawn and replenished with fresh PBS to maintain a constant volume. The samples were lyophilized, reconstituted in water, and analyzed by HPLC.

The release profile shows an initial burst release phase. Approximately a quarter of the loaded ERY was released during the first day (Fig. 11a). The burst release may be due

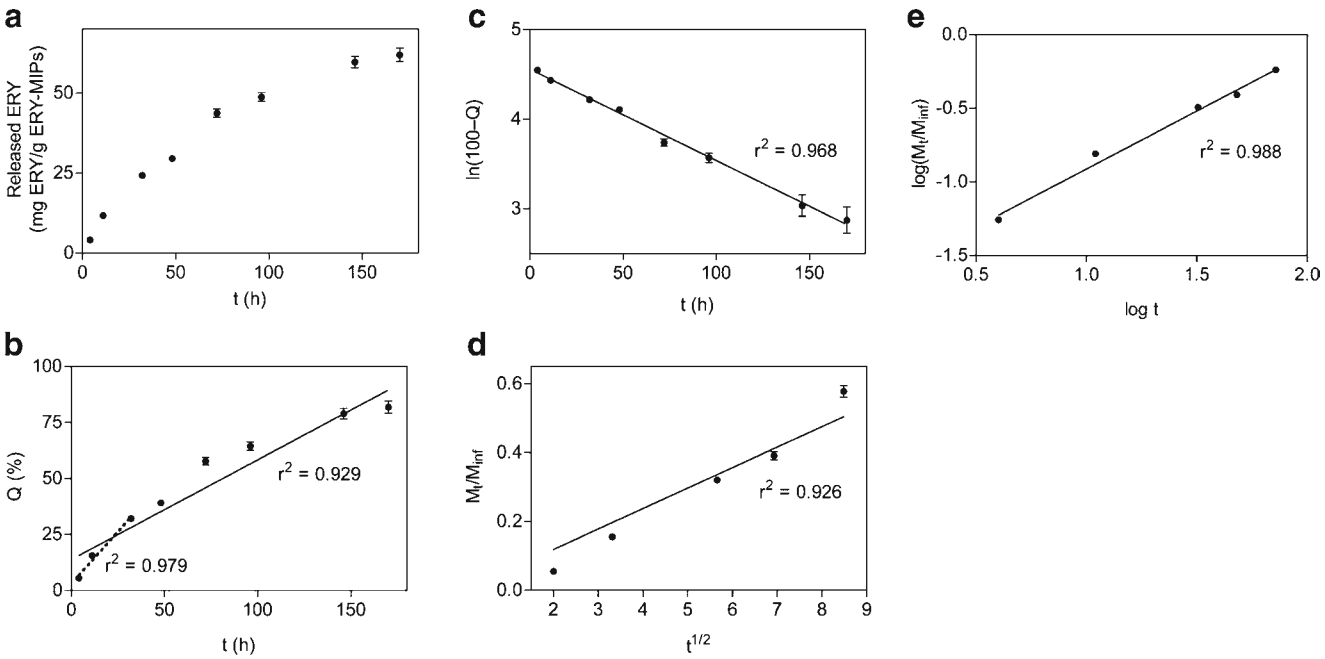

Fig. 11 (**a**) *In vitro* release profile of ERY from ERY-MIP nanocarriers (prepared with an MAA/ERY ratio of 8) in PBS (pH 7.4) at ambient temperature. (**b**) Zero-order kinetic model (dotted line includes burst phase data; solid line includes all data points). (**c**) First-order kinetic model. (**d**) Higuchi kinetic model. (**e**) Korsmeyer-Peppas (power-law) kinetic model. Error bars denote standard errors.

to loosely adsorbed drug molecules. A moderate burst release may be beneficial to provide an initial higher dose at the start of an antibiotic drug therapy. During the next 2 days, another quarter of the drug was released from the nanocarriers. After a week, 82% (corresponding to 62 mg of ERY per gram of nanocarriers) of the initially loaded ERY had been released. Drug loading was tested also in 80% aqueous methanol. The solubility of ERY was higher in this solvent mixture than in PBS, allowing a more concentrated ERY solution (*i.e.*, 7 mM) to be used for the loading step. Under these conditions, 196 mg of ERY per gram of nanocarriers was loaded with a loading efficiency of 29%. During release into PBS, approximately half of the ERY loaded under these conditions was released during the first week (Fig. S1 in Supplementary Materials). The release profiles compare well with other MIP systems studied. For example, Mirzaei *et al.* reported recently that tetracycline-imprinted *poly* (MAA–*co*–EDMA) nanoparticles in the size range 200–400 nm released 35–40% of loaded drug during the first 20 h; no further release was noted beyond this time point (22). Shi *et al.* recently reported that gatifloxacin-imprinted *poly* (MAA–*co*–EDMA) uniform nanoparticles (d=136.0±8.1 nm) released around 50% of loaded drug during the first 24 h (23).

The release kinetics was evaluated by fitting release kinetic models to the experimental release data. The burst phase of the release followed fairly well a zero-order model [$Q=Q_0+k_0t$; where Q and Q_0 are the cumulative percentage of drug released at times zero and t, respectively, and k_0 is the zero-order rate constant] (Fig. 11b). When later time points were included, a first-order model [$\ln (Q–100)=\ln Q_0 - k_1t$; where k_1 is the first-order rate constant] provided a better fit than the zero-order model (Fig. 11b and c). The Higuchi model [$M_t/M_{inf}=k_Ht^{1/2}$; where M_t and M_{inf} are the cumulative amount of drug released at time t and infinite time, respectively, and k_H is the rate constant] and the Korsmeyer-Peppas (power-law) model [$M_t/M_{inf}=k_Pt^n$; where n is the diffusional release exponent and k_P is the rate constant] were applied to $M_t/M_{inf}<0.6$ (Fig. 11d and e). In the calculations, it was assumed that M_{inf} was equal to the amount of drug loaded into the nanocarriers at time zero. The Korsmeyer-Peppas model provided a better fit than the Higuchi model. The diffusional release exponent (n) was determined to be 0.79, indicating non-Fickian diffusion.

CONCLUSIONS

Comparisons of ERY-imprinted nanocarriers with corresponding control nanocarriers, *i.e.*, non-imprinted and Boc-Phe-OH-imprinted nanocarriers, showed that the presence of ERY during the polymerization had an influence on both the morphology of the particles formed and their binding capacity of ERY. Although the ERY-MIP nanocarriers had a larger surface area than the control nanocarriers, this did not appear to be the sole cause of the higher ERY-binding capacity. A binding model generated by multivariate data analysis of binding data and molecular descriptors of a small drug library

showed that the binding of ERY to the ERY-imprinted nanocarriers was higher than expected from its molecular descriptors. The binding of ERY to the control nanocarriers, on the other hand, was explained well by the generated model.

The ERY-nanocarriers provided sustained release of ERY over a prolonged time period. We envision that these nanocarriers potentially may be useful as inclusions in bone cements, wound dressings, or implant coatings to promote sustained antibiotic and/or anti-inflammatory effects.

ACKNOWLEDGMENTS AND DISCLOSURES

This work was supported by Greta och Johan Kocks Stiftelser, Stiftelsen Syskonen Svenssons fond för Medicinsk forskning, and Magnus Bergvalls Stiftelse. Dr. Eric Carlemalm and Ms. Birgitta Lindén is acknowledged for help with TEM and BET analysis, respectively.

REFERENCES

1. Xu Z-Q, Flavin MT, Eiznhamer DA. Macrolides and ketolides. In: Dougherty TJ, Pucci MJ, editors. Antibiotic Discovery and Development. New York: Springer; 2012. p. 181–228.
2. Kanoh S, Rubin BK. Mechanisms of action and clinical application of macrolides as immunomodulatory medications. Clin Microbiol Rev. 2010;23(3):590–615.
3. Fumimori T, Honda S, Migita K, Hamada M, Yoshimuta T, Honda J, *et al.* Erythromycin suppresses the expression of cyclooxygenase-2 in rheumatoid synovial cells. J Rheumatol. 2004;31(3):436–41.
4. Ren W, Blasier R, Peng X, Shi T, Wooley PH, Markel D. Effect of oral erythromycin therapy in patients with aseptic loosening of joint prostheses. Bone. 2009;44(4):671–7.
5. Suzuki J, Ogawa M, Hishikari K, Watanabe R, Takayama K, Hirata Y, *et al.* Novel effects of macrolide antibiotics on cardiovascular diseases. Cardiovasc Ther. 2012;30(6):301–7.
6. Shinkai M, Henke MO, Rubin BK. Macrolide antibiotics as immunomodulatory medications: Proposed mechanisms of action. Pharmacol Ther. 2008;117(3):393–405.
7. Augustine JJ, Bodziak KA, Hricik DE. Use of sirolimus in solid organ transplantation. Drugs. 2007;67(3):369–91.
8. Ruygrok PN, Muller DW, Serruys PW. Rapamycin in cardiovascular medicine. Int Med J. 2003;33(3):103–9.
9. Bosnjakovic A, Mishra MK, Ren W, Kurtoglu YE, Shi T, Fan D, *et al.* Poly (amidoamine) dendrimer-erythromycin conjugates for drug delivery to macrophages involved in periprosthetic inflammation. Nanomedicine. 2011;7(3):284–94.
10. Doadrio JC, Sousa EMB, Izquierdo-Barb I, Doadrio AL, Perez-Pariente J, Vallet-Regí M. Functionalization of mesoporous materials with long alkyl chains as a strategy for controlling drug delivery pattern. J Mater Chem. 2006;16(5):462–6.
11. Portilla-Arias JA, Camargo B, García-Alvarez M, de Ilarduya AM, Muñoz-Guerra S. Nanoparticles made of microbial poly(γ-glutamate)s for encapsulation and delivery of drugs and proteins. J Biomat Sci. 2009;20(7–8):1065–79.
12. Alexander C, Andersson HS, Andersson LI, Ansell RJ, Kirsch N, Nicholls IA, *et al.* Molecular imprinting science and technology: a survey of the literature for the years up to and including 2003. J Mol Recognit. 2006;19(2):106–80.
13. Kempe H, Kempe M. Molecularly imprinted polymers. In: Albericio F, Tulla-Puche J, editors. The Power of Functional Resins in Organic Synthesis. Weinheim: Wiley; 2008. p. 15–44.
14. Alvarez-Lorenzo C, Concheiro A. Molecularly imprinted materials as advanced excipients for drug delivery systems. Biotechnol Annu Rev. 2006;12:225–68.
15. Kryscio DR, Peppas NA. Mimicking biological delivery through feedback-controlled drug release systems based on molecular imprinting. AIChE J. 2009;55(6):1311–24.
16. Fernández-González A, Guardia L, Badía-Laíño R, Díaz-García ME. Mimicking molecular receptors for antibiotics – analytical implications. Trends Anal Chem. 2006;25(10):949–57.
17. Cederfur J, Pei Y, Zihui M, Kempe M. Synthesis and screening of a molecularly imprinted polymer library targeted for penicillin G. J Comb Chem. 2003;5(1):67–72.
18. Benito-Pena E, Moreno-Bondi MC, Aparicio S, Orellana G, Cederfur J, Kempe M. Molecular engineering of fluorescent penicillins for molecularly imprinted polymer assays. Anal Chem. 2006;78(6):2019–27.
19. Kempe H, Kempe M. Influence of salt ions on binding to molecularly imprinted polymers. Anal Bioanal Chem. 2010;396(4):1599–606.
20. Kempe H, Kempe M. QSRR analysis of β-lactam antibiotics on a penicillin G targeted MIP stationary phase. Anal Bioanal Chem. 2010;398(7–8):3087–96.
21. Levi R, McNiven S, Piletsky SA, Cheong S-H, Yano K, Karube I. Optical detection of chloramphenicol using molecularly imprinted polymers. Anal Chem. 1997;69(11):2017–21.
22. Mirzaei M, Najafabadi SAH, Abdouss M, Azodi-Deilami S, Asadi E, Hosseini MRM, *et al.* Preparation and utilization of microporous molecularly imprinted polymer for sustained release of tetracycline. J Appl Poly Sci. 2013;128(3):1557–62.
23. Shi Y, Lv H, Lu X, Huang Y, Zhang Y, Xue W. Uniform molecularly imprinted poly (methacrylic acid) nanospheres prepared by precipitation polymerization: the control of particle features suitable for sustained release of gatifloxacin. J Mater Chem. 2012;22(9):3889–98.
24. Siemann M, Andersson LI, Mosbach K. Separation and detection of macrolide antibiotics by HPLC using macrolide-imprinted synthetic polymers as stationary phases. J Antibiot. 1997;50(1):89–95.
25. Song S, Wu A, Shi X, Li R, Lin Z, Zhang D. Development and application of molecularly imprinted polymers as solid-phase sorbents for erythromycin extraction. Anal Bioanal Chem. 2008;390(8):2141–50.
26. Geng L, Kou X, Lei J, Su H, Maa G, Su Z. Preparation, characterization and adsorption performance of molecularly imprinted microspheres for erythromycin using suspension polymerization. J Chem Technol Biotechnol. 2012;87(5):635–42.
27. Kou X, Lei J, Geng L, Deng H, Jiang Q, Zhang G, *et al.* Synthesis, characterization and adsorption behavior of molecularly imprinted nanospheres for erythromycin using precipitation polymerization. J Nanosci Nanotechnol. 2012;12(9):7388–94.
28. Zhang Z, Yang X, Zhang H, Zhang M, Luo L, Hu Y, *et al.* Novel molecularly imprinted polymers based on multi-walled carbon nanotubes with binary functional monomer for the solid-phase extraction of erythromycin from chicken muscle. J Chromatogr B. 2011;879(19):1617–24.
29. Kempe M, Mosbach K. Receptor binding mimetics: a novel molecularly imprinted polymer. Tetrahedron Lett. 1995;36(20):3563–6.
30. Kempe M. Antibody mimicking polymers as chiral stationary phases in HPLC. Anal Chem. 1996;68(11):1948–53.
31. Ye L, Cormack PAG, Mosbach K. Molecularly imprinted monodisperse microspheres for competitive radioassay. Anal Commun. 1999;36(2):35–8.
32. Connolly ML. Computation of molecular volume. J Am Chem Soc. 1985;107(5):1118–24.

33. Sibrian-Vazquez M, Spivak DA. Molecular imprinting made easy. J Am Chem Soc. 2004;126(25):7827–33.
34. Ray RS, Mehrotra S, Shankar U, Suresh Babu G, Joshi PC, Hans RK. Evaluation of UV-induced superoxide radical generation potential of some common antibiotics. Drug Chem Toxicol. 2001;24(2): 191–200.
35. Jedliński Z, Paprotny J. Synthesis and polymerisation of some N-alkylolacryl-amides. III. Polymerization of 2-methacrylamido-2-methyl-propanediol-l,3 and 2-methacrylamido-2-methylpropanol-1. J Polym Sci Part A-1. 1967;5(11):2957–60.
36. Karlsson JG, Karlsson B, Andersson LI, Nicholls IA. The roles of template complexation and ligand binding conditions on recognition in bupivacaine molecularly imprinted polymers. Analyst. 2004;129(5):456–62.
37. Zhang Y, Song D, Lanni LM, Shimizu KD. Importance of functional monomer dimerization in the molecular imprinting process. Macromolecules. 2010;43(15):6284–94.
38. Cacho C, Turiel E, Martin-Esteban A, Pérez-Conde C, Cámara C. Characterisation and quality assessment of binding sites on a propazine-imprinted polymer prepared by precipitation polymerization. J Chromatogr B. 2004;802(2):347–53.
39. Chen Z, Ye L. Controlling size and uniformity of molecularly imprinted nanoparticles using auxiliary template. J Mol Recognit. 2012;25(6):370–6.